Journal of Materials Chemistry B

Accepted Manuscript

ROYAL SOCIETY OF CHEMISTRY

www.rsc.org/materialsB

Nanoscale Control of Silks for Nanofibrous Scaffold Formation with Improved Porous Structure

Shasha Lin[a], Guozhong Lu[b,#], Shanshan Liu[a], Shumeng Bai[a], Xi Liu[a], Qiang Lu[a,c,*], Baoqi Zuo[a,*], David L. Kaplan[d] and Hesun Zhu[e]

[a]*National Engineering Laboratory for Modern Silk, College of Textile and Clothing Engineering, Soochow University, Suzhou 215123, People's Republic of China*

[b]*Department of Burns and Plastic Surgery,The Third Affiliated Hospital of Nantong University, Wuxi 214041, People's Republic of China*

[c]*Jiangsu Province Key Laboratory of Stem Cell Research, Medical College, Soochow University, Suzhou 215006, People's Republic of China*

[d]*Department of Biomedical Engineering, Tufts University, Medford, MA 02155, USA*

[e]*Research Center of Materials Science, Beijing Institute of Technology, Beijing, 100081, People's Republic of China*

Corresponding authors:

Qiang Lu, Tel: (+86)-512-67061649; E-mail: Lvqiang78@suda.edu.cn

Baoqi Zuo, E-mail: bqzuo@suda.edu.cn

The author has same contribution with the first author

Abstract

Silk-based porous scaffolds have been used extensively in tissue engineering because of their excellent biocompatibility, tunable biodegradability and robust mechanical properties. Although many silk-based scaffolds have been prepared through freeze-drying, a challenge remains to effectively control porous structures during this process. In the present study silk fibroin with different nanostructures were self-assembled in aqueous solution by repeated drying-dissolving process and then used to improve porous structure formation in lyophilization process. Viscosity, secondary structures and water interactions were also studied to exclude their influence on the formation and control of porous structures. Following nanofiber formation in aqueous solution, silk scaffolds with improved porous structure were directly formed after lyophilization and then stabilized with water or methanol annealing treatments. Compared to silk scaffolds derived from fresh solution, the nanofibrous scaffolds showed significantly better cell compatibility *in vitro*. Therefore, this nanoscale control of silk offers feasible way to regulate the matrix features including porous structure and nanostructure, which are important in regulating cell and tissue outcomes in tissue engineering and regeneration, and then achieve silk-based scaffolds with improved properties.

Keywords: Silk; Scaffolds; Porous structure; Tissue engineering; Nanostructure

1. Introduction:

Compared to other proteins or non-biological materials, silk fibroin not only has good biocompatibility, but also shows better mechanical properties, lower inflammatory reaction, and controllable degradation behaviors.[1-8] Recently, silk fibroin has been extensively used as matrices for different kind of cell cultures and as scaffolds for various tissue regenerations such as skin, nerve, bone, cartilage and blood vessel. [1-8] However, a challenge for scaffold fabrication remains to further improve silk biocompatibility and inductivity for different tissue regeneration needs. [9-13] Although growing studies indicated that mimicking microporous and nanofibrous structures of extracellular matrix (ECM) could further improve the biocompatibility of different biomaterials, [14-18] there is no effective way to fabricate silk scaffolds with suitable microporous and nanofibrous structures simultaneously.

For different biomedical applications, one basic step is fabricating suitable porous structure to provide enough surface area for cell growth and tissue regeneration. The controlled release of different drugs and growth factors from the scaffolds was sometimes necessary for regulating different tissue regenerations. Silk-based scaffolds have been prepared through a number of methods in which salt leaching and freeze-drying are the most widely used.[19-21] Different silk-based drug release systems including scaffold system have also been designed to achieve sustained release of different drugs without significant loss of drug activity since silk fibroin had better ability to maintain activity and function of sensitive drugs such as enzymes and growth factors than other synthetic and natural biomaterials.[19-21] Unfortunately, high concentrations of salt used in salt-leaching process prevent silk-based scaffolds from harboring labile drugs or growth factors, or the formation of nanofibrous structures with low β-sheet content. Freeze-drying method is economical and controllable way of preparing porous structures of different biomaterials in which the size and structure of micropores could be easily regulated by adjusting polymer

concentration or freezing temperature.[22, 23] It is also a popular way to maintain the activity of different growth factors in preparation process. Therefore, freeze-dried silk-based scaffolds have promising future not only in ECM-mimic fabrication, but also in the incorporation and release of sensitive drugs or growth factors, which would provide better microenvironment for different tissue regenerations. However, although powerful and effective for designing many natural or synthetic biomaterial scaffolds, the freeze-drying method remains a challenge for forming suitable porous scaffolds from pure regenerated silk fibroin solution. The freeze-dried silk fibroin scaffolds, usually composed of separate layers, showed very fragile mechanical properties that can't satisfy minimum requirements for most of tissue repairs. Different ways including cross-linking or blending with other natural or synthetic polymers were also used to improve porous structure formation of silk-based scaffolds following possible sacrifice of good biocompatibility.[24-26] Although preparing freeze-dried scaffolds with suitable porous structure is difficult for regenerated silk fibroin, excellent porous scaffolds could be easily achieved by directly freeze-drying natural silk dopes. [27] The finding implies that there are undiscovered factors in regulating porous structure formation for freeze-dried silk fibroin scaffolds. Elucidating these factors would be critical for designing and preparing silk fibroin scaffolds with desired porous structures and even suitable drug release behaviors, and then improve the following applications in different biomedical fields.

In our previous study, collagen was used to control silk fibroin self-assembly for facilitating porous scaffold formation through lyophilization. [23] An improved porous structure was achieved following nanofiber formation, implying a critical effect of silk nanofiber on porous structure formation. [23] Therefore, preparing silk nanofibers in aqueous solution might be pivotal for understanding the effect of nanostructure on scaffold fabrication and then designing silk scaffolds with improved porous structures. A slow self-assembling process from nanoparticles to nanofibers has been found for silk fibroin. [28] Although the process could be regulated by different factors such as

time, temperature and charge, the nanofiber formation was accompanied with the transformation from random structure to water-stable silk I or silk II crystals, resulting in a failure to maintain nanofiber structure in aqueous solution.[28, 29] Recently, a repeated quickly drying-dissolving process was used to prepare metastable silk nanoparticles. The nanoparticles easily transformed into soluble amorphous nanofibers in diluted aqueous solutions (about 0.3 wt%) after cultured for above 12 hours at 25°C. Further study revealed that the amorphous silk nanofibers gradually transformed into silk II nanofibers, resulting in hydrogel formation.[30] Considering the difference of concentrating times between the slow and quickly drying-dissolving processes, we suggested that decreasing the drying rate in the repeated quickly drying-dissolving process might directly result in soluble silk nanofiber formation in suitable concentrations (1-4 wt%). If so, the effect of silk nanofibers on porous structure formation would be elucidated, and then silk fibroin scaffolds composed of ECM-mimic nanofibrous and microporous structures can be directly prepared from silk nanofiber solution after lyophilization. Therefore, in the present research, a series of silk fibroin solutions containing different contents of silk nanofibers were prepared in order to elucidate their influence on porous structure formation. The *in vitro* cell culture on the nanofibrous scaffolds was also studied, showing significant improvement of biocompatibility.

2. Experimental Section

2.1 Preparation of silk fibroin solutions

B. mori silk fibroin solutions were prepared according to our previous published procedures. [29] Cocoons were boiled for 20 min in an aqueous solution of 0.02 M Na_2CO_3 and then rinsed thoroughly with distilled water to extract the sericin proteins. After drying the extracted silk fibroin was dissolved in 9.3M LiBr solution at 60°C for 4 h, yielding a 20% (w/v) solution. This solution was dialyzed against distilled water using dialysis tube (MWCO 3500) for 72 h to remove the salt. Then the solution was centrifuged at 9000 r/min for 20 min at 4°C to remove silk

aggregations formed during the process. The final concentration of silk in water was about 6%, determined by weighing the remaining solid after drying.

2.2 Silk nanofiber formation in aqueous solution

Silk fibroin with different nanostructures was prepared by an improved repeated drying-dissolving process. Silk fibroin solutions (6%, 5 ml) were cast on polystyrene Petri dishes (diameter 90 mm) and dried at room temperature for about 12 h with controlled drying rate. Once the dried silk fibroin films formed, they were added in 5 ml distilled water and re-dissolved under stirring speed of 300 rpm for 1 h to generate silk fibroin solutions at room temperature, termed SF-1. Then the drying-dissolving process was repeated to generate solutions SF-2, SF-3 and SF-4. The nanostructures of silk fibroin were measured after every drying-dissolving cycle process. After four cycles, most of silk fibroin has assembled into short nanofibers in aqueous solution. As control, silk fibroin solution without this drying-dissolving treatment was prepared and is termed SF-0. All the solutions were diluted to 3% with water for lyophilization.

2.3 Morphological and structural properties of silk fibroin in aqueous solution

The morphology of silk fibroin in aqueous solution was observed by AFM (Veeco, Nanoscope V, Plain view, NY, America) in air. A 225 μm long silicon cantilever with a spring constant of 3 Nm^{-1} was used in tapping mode at 1.5 Hz scan rate. To prepare the samples for AFM imaging, different SF solutions were diluted to below 0.0001 wt% with deionized water. [30] Once diluted, 2 μl of the diluted SF solution was quickly dropped onto freshly cleaved 4×4 mm^2 mica surfaces and dried under a nitrogen gas. Above 50 different areas of each sample were investigated to achieve reasonable structures of silk fibroin. Images were processed with Nanoscope Analysis software (Bruker, Germany) to remove background slope. The contour length of silk fibroin nanofiber was measured using Image-ProPlus software v.6.0 (Media Cybernetics,USA).

Secondary structures of silk fibroin in the different solutions were studied with circular dichroism (CD) spectrometer. CD spectra were recorded on a spectrophotometer (Model 410, AVIV, Lakewood, America) equipped with a Peltier temperature controller. Spectra were obtained from 250 to 190 nm at a scanning speed of 10nm/min at 25 ^{o}C. The CD spectra represented the average of three measurements and were smoothed. CD data are reported as mean residue ellipticity ([Θ], degree·cm^{2}·dmol^{-1})

Rheological studies of different silk fibroin solutions were run on a Rheometer (AR2000, TA Instruments, New Castle, USA) with a 35 mm cone plate (Ti, 35/1°). The normal force applied on the sample during lowering of the top plate was limited to 0.1 N. The shear rate was linearly increased from 0.01 to 5000 s^{-1} at 25^{o}C.

2.4 Scaffold formation

1 ml of different silk solutions with concentration of 3% (SF-0, SF-1, SF-2, SF-3, SF-4) were poured into cylindrically-shaped container and placed at -20°C. The freezing rate kept 0.125°C/s to make sure that all the solutions transformed into ice solid after 24 h. Then the frozen silk solutions were lyophilized at -50^{o}C for about 72 h. After lyophilization, the scaffolds were prepared and termed SF-0-S, SF-1-S, SF-2-S, SF-3-S, SF-4-S, respectively. Then water-insoluble scaffolds were achieved by water annealing[23, 31] or methanol annealing treatments.[22] Briefly, different scaffolds were placed on a removable platform under which water was filled in a desiccator with a 25 in. Hg vacuum for 6 h in water annealing process while immersed in 80% (v/v) methanol for 30 min in methanol annealing process to induce crystallization.

2.5 Scanning electron microscopy (SEM) of the scaffolds

The morphology of the scaffolds was observed using a SEM (Hitachi S-4800, Hitachi, Tokyo, Japan). Samples were mounted on a copper plate and sputter-coated with gold layer with 20-30 nm thick prior to imaging. Since

previous study has indicated that the nanoscale architectures of silk fibroin are usually covered by compact surface of the pore walls,[23] 40 mg of different methanol-treated scaffolds were incubated at 37°C in 40 ml phosphate saline (PBS) containing 5 U/ml protease XIV for 8 h to degrade the compact surface. Then the morphologies of the different scaffolds after degradation were examined using a Hitachi S-4800 SEM (Model S-4800, Hitachi, Tokyo, Japan). The wall thickness and pore size of scaffolds was measured using Image-ProPlus software v.6.0 (Media Cybernetics, USA). Above 50 different sites for every sample were measured and then the average values were achieved.

2.6 Structural analysis of the scaffolds

The structure of the different scaffolds was analyzed by FTIR on a NICOLET FTIR 5700 spectrometer (Thermo Scientific, FL, USA). Approximately 1 mg of the freeze-dried samples was pressed into a pellet with 200 mg of potassium bromide. For each measurement 64 scans were coded at a resolution of 4 cm^{-1}, with the wave number ranging from 400-4000 cm^{-1}.[32]

To investigate the structure and crystallinity of the different scaffolds, XRD experiments were also performed with an X-ray diffractometer (X′Pert-Pro MPD, PANalytical B.V. Holland) using CuKa radiation. Irradiation conditions were at 40 kV and 30 mA and a scanning rate of 0.6°/min.

2.7 Differential scanning calorimetry (DSC)

The interaction between silk fibroin and water in different lyophilized scaffolds was measured in a TA instrument Q100 DSC (TA instruments, New Castle, DE) under a dry nitrogen gas flow of 50 ml min^{-1}. In order to remove the influence of free water, temperature-modulated differential scanning calorimetry (TMDSC) measurements were performed using a TA instrument Q100 equipped with a refrigerated cooling system. The samples were heated at

$2^{o}C\ min^{-1}$ from -30 to 250°C with a modulation period of 60 s and a temperature amplitude of 0.318°C. Only bound water peaks could appear in the TMDSC curves based on our previous study. [31]

2.8 Cell culture

Considering amniotic fluid-derived stem cells (AFSCs) with a capacity to differentiate into multiple cells and avoid ethical concerns with embryonic stem cells have been used in different tissue regeneration applications, [33-36] amniotic fluid-derived stem cells were used to evaluate the cytocompatibility of the scaffolds. Samples of amniotic fluid were obtained from the First Affiliated Hospital of Soochew University (Suzhou, Jiangsu, China) following routine amniocentesis carried out on pregnant women at 15 to 35 weeks of gestation. All the procedures were performed following the guidelines established by the First Affiliated Hospital of Soochew University and the First Affiliated Hospital of Soochew University Ethics Committee; a written consent was obtained from each woman to use the amniotic fluid for research purposes. The isolation of human amniotic fluid-derived stem cells has been described previously.[37] Amniotic fluid-derived stem cells were cultured in α-Modified Eagle Medium (α-MEM) supplemented with 10% fetal bovine serum (FBS), 1% UI/ml Streptomycin-Penicillin (all from Invitrogen, Carlsbad, CA) and growth factor: Basal, C Frozen Supplement (Irvine Scientific, Santa Ana, CA). The medium was replaced every 2 d and the cultures were maintained in a humidified incubator at 37°C and 5% CO_2. The scaffolds (thickness 2 mm) were punched into small discs with a diameter of 5 mm and then sterilized by γ radiation. After pre-conditioning with the culture medium overnight, the samples were transferred into a non-treated 6-well cell culture plate and seeded with the amniotic fluid-derived stem cells at the density of 1×10^5/well.

2.9 Cell growth and morphology

The cell morphology of the amniotic fluid-derived stem cells on the scaffolds was examined by confocal microscopy. Briefly, the cell-seeded scaffolds were washed three times with PBS (pH7.4). Cells were fixed for 30 min by incubating in 4% paraformaldehyde, followed by further washing. The cells were permeabilized using 0.1% Triton X-100 for 5 min and incubation with FITC-phalloidin for 20 min at room temperature, then PBS washing and finally staining with 4, 6-diamino-2-phenyl indole (DAPI) for 1 min. Fluorescence images from stained samples were obtained through a confocal laser scanning microscope (CLSM, Olympus FV10 inverted microscope, Nagano, Japan). The cell morphology on the scaffolds was confirmed by SEM. After harvest, the seeded scaffolds were washed with PBS 3 times and fixed in 4% paraformaldehyde (Sigma-Aldrich, St. Louis, Mo) at room temperature, and then the scaffolds were washed 3 times with PBS again. Fixed samples were dehydrated through a gradient of alcohol (50%, 70%, 80%, 90%, 100%, 100%) followed by lyophilization. Specimens were examined using a Hitachi Model S-4800 SEM (Hitachi, Tokyo, Japan).

2.10 DNA content

To study cell proliferation on the scaffolds, samples were harvested at the indicated time point (from day 1 to day 12), and digested with proteinase K overnight at 56°C, as described previously. [38] The DNA content was determined by using Pico Green TM DNA assay following the protocols of the manufacturer (Molecular Probes, Eugene, OR). Samples (n=5) were measured at excitation wavelength of 480 nm and emission wavelength of 530 nm using a BioTec Synergy 4 spectrofluorometer (BioTec, Winooski, UK). The amount of DNA was calculated by interpolation from a standard curve prepared with lambda DNA in 10×10^{-3} M Tris-HCl (pH7.4), 5×10^{-3} M NaCl, 0.1×10^{-3} M EDTA over a range of concentrations.

2.11 Statistical analysis

All the morphological and structural experiments were run in triplicate and the typical results were present in the present study. All the cell proliferation experiments were also run in quintuple and results are expressed as mean ± standard deviation for n = 5. Statistical analysis of data was examined by one-way ANOVA and a post host-test. Differences between groups of $P < 0.05$ were considered statistically significant.

3. Results and Discussion

3.1 Nanofiber formation of silk fibroin in aqueous solution

Our previous study has found a time-depending nanoparticle-nanofiber assembling process for silk in aqueous solution that regulated by different factors such as concentration, temperature, pH and charge.[28] Based on the study, silk fibroin films composed of nanofibers were directly prepared by a slow concentration process following secondary structure transformation from random to silk I. [38] Unfortunately, the silk fibroin nanofibers composed of silk I structure cannot re-dissolve in aqueous solution, failing to form porous scaffold. More recently, a repeated drying-dissolving process was used to prepare nanoparticles with size of above 100 nm. The particles could easily be transformed into nanofibers in low concentration at different temperatures without un-soluble silk fibroin formation.[28] However, the concentration of the nanofiber solution was generally below 0.3%, unsuitable for porous scaffold preparation.

Although the above studies don't provide feasible nanofiber solutions for scaffold preparation, they imply a possibility to accelerate nanoparticle-nanofiber transition rate in a drying-dissolving process but delay silk I or silk II formation happened in slow drying process through further regulating different factors such as drying rate. Therefore, in the present study, an improved drying-dissolving cycle was used to influence the nanostructures of silk fibroin, avoiding silk I and silk II formation in aqueous solution. Drying rate, lower than that in our previous

drying-dissolution cycle [29] but faster than that in silk I and silk II formation process, [30] was used to facilitate nanofiber formation. The concentration of silk fibroin maintained 6% in the drying-dissolving cycles. As shown in Fig. 1 (a, c, e, g, i), silk fibroin solutions with different contents of nanofibers were prepared by the repeating drying-dissolving process. Silk fibroin was mainly composed of nanospheres with sizes about 20-40 nm in diameter in solution. After one drying-dissolving cycle, the silk fibroin nanostructures slightly changed. A few short nanofibers with diameter of about 20 nm and length of about 100 nm appeared in solution. The content of nanofibers increased following the repeated drying-dissolving cycles. After the cycles were repeated three times, most of silk fibroin had aggregated from nanospheres to nanofibers. And then, the short fibers assembled into longer nanofibers with length range from 100 nm to 500 nm. Therefore, silk fibroin with different nanostructures were prepared in solution through this simple cycling process, providing a useful processing route to investigate the influence of nanostructures on scaffold formation.

3.2 Microstructure control of silk fibroin scaffolds

Silk fibroin scaffolds were then prepared from the above solutions through lyophilization (Fig.1b, d, f, h, j). When silk fibroin maintained nanosphere structure in aqueous solution, separate sheet rather than porous structure formed in the freeze-dried scaffolds (SF-0-S, SF-1-S). Following gradual nanofiber formation in the aqueous solution, the scaffold microstructure gradually changed from lamellar (SF-2-S) to interconnected porous structures (SF-3-S and SF-4-S) with pore size of above 200 μm, following with the thickness decrease of pore walls from 4.3 μm to 1.2 μm. After water-annealing or methanol annealing treatments, the scaffolds maintained their respective lamellar or porous structures (data not shown), indicating the trivial influence of post-treatments on scaffold microstructures. Since the nanoscale architectures of silk fibroin are generally covered by compact surface.[23] the methanol-treated scaffolds were cultured in protease XII solution for 8 hours to degrade the surface. As shown in

Fig. 2, more nanofibrous structures were observed in the scaffolds derived from solution with added nanofibers, implying that the nanoscale and microscale microstructures of silk fibroin scaffolds could be influenced by silk fibroin nanostructures in solution.

The nano-structural changes of silk fibroin in solution also resulted in marked variation of other solution properties that might be further affect porous structures of the freeze-dried scaffolds, so different factors such as secondary structure, silk fibroin-water interactions and viscosity were investigated. The secondary structures of silk fibroin in aqueous solutions were investigated by CD. As shown in Fig. 3, after different drying-dissolving processes, silk fibroin still maintained random structure in water without significant conformation changes. Considering that the nanostructures gradually changed following the drying-dissolving processes, CD results implied that silk fibroin composed of different nanostructures should also keep random structure in aqueous solutions. Then the secondary and crystal structures of lyophilized scaffolds derived from the solutions were studied by FTIR and XRD (Fig. 4). The infrared spectral region within 1700-1500 cm^{-1} is assigned to absorption by the peptide backbones of amide I (1700-1600 cm^{-1}) and amide II (1600-1500 cm^{-1}), which have been commonly used for the analysis of different secondary structures of silk fibroin. [29] The peaks at 1630-1645 cm^{-1} (amide I) and 1520-1540 cm^{-1}(amide II) are characteristic of random coil. [39] In the present study the amide I and amide II bands for all the scaffolds showed strong peaks at 1645 cm^{-1} and 1535 cm^{-1}, indicating that silk fibroin maintained random structures in all the lyophilized scaffolds (Fig. 4A). The secondary and crystal structures of the scaffolds were further supported with XRD curves (Fig. 4B). The peaks in the range of 5-40^{o} are usually used to study the crystal structures of silk fibroin since all the main crystal peaks appear in the range. [40-42] All the scaffolds showed an amorphous state, characterized by the presence of a broad peak in the 2θ scattering angle range from 10^{o} to 35^{o}. [43] XRD is generally used to investigate crystal structures rather than amorphous states of different materials. In this study, although

wider peak appeared following the increase of silk nanofibers in solutions, it is impossible to compare amorphous structure changes from XRD curves. Since silk fibroin with different nanostructures had similar random secondary structure before and after scaffold formation, the secondary structure of silk fibroin had no significant effect on porous structure formation.

Our previous results have revealed that the interaction between silk fibroin and water could be studied through temperature-modulated differential scanning calorimetry (TMDSC).[44] The definition of bound water in silk has been a topic of discussion for many years. The origin of the large endothermic peak in normal DSC curves of silk materials (Fig S1), ranging from 80 to 150^{o}C, was once considered to be directly contributed by the melting of bound water in some groups [45] while other groups believed that this peak was just the experimental sign of the water loss including free and bound water. [46] In order to exclude the effect of free water during the normal heat ramping process, Hu et al developed a TMDSC process to distinguish the influence of bound water from normal DSC. [47, 48] Based on their study, the endothermic peak between 50-100^{o}C in TMDSC curves of silk was related to the bound water in silk and used to estimate the strength of water-silk fibroin interactions. [28, 29] Based on our previous study, [30] the nanostructure changes coupling with secondary structure transformation in the drying-dissolving cycles could influence the interaction between silk and bound water. Fig. 5A shows the reverse DSC curves for SF-0-S, SF-1-S, SF-2-S, SF-3-S, and SF-4-S. Although the influence of nanostructure on silk fibroin-water interactions still needs further investigation, different silk fibroin-water interactions appeared in the scaffolds, providing enough information to reveal the relationship between silk fibroin-water interaction and porous structure formation. Strong interactions formed in SF-1-S and SF-4-S while disappeared in SF-0-S, SF-2-S and SF-3-S. According to the AFM and SEM results, when silk fibroin assembled into nanofibers, porous structures formed even with weak silk fibroin-water interactions (SF-3-S). On the other hand, if silk fibroin was

mainly composed of nanospheres, the prepared scaffolds had lamellar structures whether strong silk fibroin-water interactions were present or not (SF-1-S and SF-0-S). The results reveal that silk fibroin-water interactions also have no significant influence on the microstructure formation of silk fibroin scaffolds. The viscosity of different solutions was also studied to elucidate the impact on porous structure formation (Fig. 5B). SF-0 and SF-1 solutions had higher viscosity at low shear rate. The solutions with higher viscosity at low shear rate formed lamellar structures, indicating a trivial effect of viscosity on porous structure formation in this study.

Since these factors including secondary structure, silk fibroin-water interactions and viscosity had no significant influence on porous structure formation, it is reasonable to believe that silk fibroin nanostructure in solution is a critical factor in the control of porous structures from the freeze-drying process. A hypothesis is proposed to explain the effect of silk fibroin nanostructures on microstructure formation of lyophilized scaffold (Fig. 6). The porous structures of silk fibroin scaffolds are related to ice growth in the freezing process. When silk fibroin is mainly composed of nanospheres or microspheres, ice easily grows and pushes silk fibroin towards sheet formation since no strong interaction/entanglement forms between the nanospheres or microspheres. Once silk fibroin assembles into nanofibers, the entanglement between the nanofibers restrains the push from ice growth, resulting in porous structure formation. The hypothesis was further supported through preparing silk fibroin nanofiber firstly and then adding them into fresh silk fibroin solution to prepare lyophilized scaffolds. Improved porous structures were directly achieved following the increase of silk fibroin nanofibers in fresh silk fibroin solution (Fig. 7), which supported that nanofiber formation was an effective way to ameliorate microstructures of lyophilized silk fibroin scaffolds. Therefore, silk fibroin porous scaffolds composed of similar nanofibrous architectures with ECM could be directly prepared in a freeze-drying process, might providing an effective way to design silk-based materials with improved biocompatibility.

3.3 Structural analysis for the post- treated scaffolds

Since freeze-dried silk fibroin scaffolds are soluble in water, it is necessary to improve their stability through different post treatments such as water annealing and methanol annealing.[31, 43] Different studies has confirmed that the characteristic amide I band for silk I structure appears at 1650 cm^{-1} and then move to 1625 cm^{-1} for silk II structure.[29, 32, 49] After methanol treatment all the scaffolds showed specific peaks for the silk II structure (1620 cm^{-1}), while silk I structures formed (1650 cm^{-1}) in the water-annealed scaffolds (Fig. 8). Although the quantitative changes of the secondary structures between different scaffolds can't be provided in the present study, the scaffolds composed of nanofibers showed similar transformational trends compared to previous silk fibroin scaffolds, [18] indicating that the existing methods of controlling the secondary structures of silk scaffolds are also effective for the nanofibrous scaffolds. Considering different ways have been developed to regulate silk secondary and crystal structures, and then resulted in different mechanical properties and degradation behaviors, [11, 18, 43, 50] it is feasible to further fabricate the properties of the nanofibrous scaffolds with different ways, providing more suitable microenvironments for specific cell and tissue. Therefore, the silk fibroin nanofiber formation in aqueous solution in combination with freeze-drying method and different post treatments offers a promising method to design silk-based scaffolds with desired microstructures and degradation behavior.

3.4 Cell compatibility

Although many different methods have been developed to prepare silk-based scaffolds, [51, 52] few studies were reported to compare the results of cell growth on these silk scaffolds. The reason is that the scaffolds prepared by different processes generally have various porous structures, nanostructures, pore size, secondary conformations, stiffness, and hydrophilic-hydrophobic properties while these different properties all have significantly influence on cell behaviors, making it impossible to achieve reasonable information about the relationship between silk

scaffold fabrication and cell compatibility. Therefore, in our present study, AFSCs were cultured on the methanol-annealed SF-0-S and SF-4-S scaffolds to elucidate the influence of microstructure fabrication on cell behaviors since the two scaffolds were derived from same silk solution and had similar secondary structures but different nanofibrous architectures and porous structures. On the other hand, mammalian cells response to lots of growth factors that regulate their function including proliferation, differentiation, and apoptosis. Both autocrine growth mechanisms (in which the individual cell synthesizes and/or secretes a substance that stimulates that same cell type to undergo a growth response) and paracrine growth mechanisms (in which the individual cells responding to the growth factor synthesize and/or secrete a substance that stimulates neighboring cells of another cell type) are important in cell growth in vivo and in vitro. The low cell seeding density would result in the decrease of concentration of substance secreted through autocrine and/or paracrine. Thus, the cells growth will be inhibited at the initial period after seeding. Considering that the excellent cell-compatibility of silk-based scaffolds generally results in over-rapid growth of cells, [32] lower initial cell seeding density compared to previous study was used to reduce the cell growth on the scaffolds.[53] DNA content results showed different cell proliferation behaviors on the two scaffolds (Fig. 9). We noted that a few cells were observed on the scaffolds within 6 days, which was due to the low initial cell seeding density. Significant higher cell numbers were found on the methanol-annealed SF-4-S scaffold after day 3. Considering the adhered cells on the two scaffolds at day 1 were almost same, the higher cell numbers on the methanol-annealed SF-4-S scaffold indicated that cells grew better on the SF-4-S scaffolds. Confocal microscopy and SEM results confirmed the better cell growth on the nanofibrous scaffolds (Fig. 10 and 11). At day 12, cells proliferated significantly and interacted to form aggregates on the nanofibrous scaffolds (Methanol-annealed SF-4-S) while maintained separate states on the lamellar scaffolds (Methanol-annealed SF-0-S). More cell-ECM monolayer structures formed on the surface of the nanofibrous scaffolds, implying better ECM formation on the scaffolds. Cell culture results indicated that the nanofibrous silk

scaffolds with good porous structure showed significant better biocompatibility than the scaffolds derived from fresh silk solution. Many studies have confirmed that ECM-mimic nanofibrous structures could provide better bionic microenvironment for cells, resulting in better cell growth *in vitro* and improved tissue regeneration *in vivo*. [14-18] Some groups also found that porous structures of the scaffolds had significant influence on cell behaviors. [54-57] In our present study, silk nanofibers were assembled in aqueous solution and then induced good porous structure formation in the freeze-dried scaffolds. Although it is impossible to clarify their specific actions of nanofibrous and microporous structures in improving the biocompatibility, the cell culture *in vitro* has validated that nanofiber assembly of silk in solution not only improved the porous structure of lyophilized scaffolds, but also provided better microenvironment for cells, which would further facilitate the applications of silk scaffolds in different tissue repairs.

Conclusions

Silk fibroin solutions with different nanostructures were prepared to regulate scaffold formation in a freeze-drying process. A hypothesis for controlling porous structures of freeze-dried silk fibroin scaffolds was elucidated, indicating that the nanostructures of silk fibroin in solution have a critical effect on scaffold formation. Combined with different post treatment methods, the lyophilization method is a useful approach to prepare silk fibroin scaffolds with controllable microstructures, which may make it possible to design silk-based scaffolds according to specific requirements for different tissues.

Acknowledgements

We thank National Basic Research Program of China (973 Program 2013CB934400, 2012CB22302), and NSFC (21174097, 81272106) for support of this work. We also thank the Priority Academic Program Development of Jiangsu Higher Education Institutions (PAPD), the Excellent Youth Foundation of Jiangsu Province(BK2012009),

the NIH (EB002520)), and the Key Natural Science Foundation of the Jiangsu Higher Education Institutions of China (11KGA430002) for support of this work.

References

1 B. Kundu, R. Rajkhowa, S. Kundu, C. Subhas and X. Wang, *Adv Drug Deliver Rev.*, 2013, **65**, 457-470.

2 D. Y. Yao, S. Dong, Q. Lu, X. Hu, D. L. Kaplan, B. B. Zhang and H. S. Zhu, *Biomacromolecules*, 2012, **13**, 3723-3729.

3 C. Correia, S. Bhumiratana, L. P.Yan, A. L. Oliveira, J. M. Gimble, D. Rockwood, D. L. Kaplan, R. A. Sousa, R. L. Reis and G. Vunjak-Novakovic, *Acta Biomater.*, 2012, **8**, 2483-2492.

4 N. Kasoju and U. Bora, *Adv Healthcare Mater.*, 2012, **1**, 393-412.

5 G. H. Altman, F. Diaz, C. Jakuba, T. Calabro, R. L. Horan, J. S. Chen, H. Lu, J. Richmond and D. L. Kaplan, *Biomaterials*, 2003, **24**, 401-416.

6 Y. F. Zhang, W. Fan, Z. C. Ma, C. T. Wu, Fang, W. G. Liu and Y. Xiao, *Acta Biomater.*, 2010, **6**, 3021-3028.

7 Y. Wang, E. Bella, C. S. D. Lee, C. Migliaresi, L. Pelcastre, Z. Schwartz, B. D. Boyan and A. Motta, *Biomaterials*, 2010, **31**, 4672-4681.

8 S. Huang and X. B. Fu, *J Control Release*, 2010, **142**, 149-159.

9 D. G. Harkin, K. A. George, P. W. Madden, I. R. Schwab, D. W. Hutmacher and T. V. Chirila, *Biomaterials*, 2011, **32**, 2445-2458.

10 R. Rajkhowa, E. S. Gil, J. Kluge, K. Numata, L. J. Wang, X. G. Wang and D. L. Kaplan, *Macromol Biosci.*, 2010, **10**, 599-611.

11 S. Das, F. Pati, S. Chameettachal, S. Pahwa, A. R. Ray, S. Dhara, S. Ghosh, *Biomacromolecules*, 2013, **14**, 311-321.

12 L. S. Wray, J. Rnjak-kovacina, B. B. Mandal, D. F. Schmidt, E. S. Gil and D. L. Kaplan, *Biomaterials*, 2012, **33**, 9214-9224.

13 D. M. Lin, H. Tao, J. Trevino, J. P. Mondia, D. L. Kaplan, F. G. Omenetto and L. Dal Negro, *Adv Mater.*, 2012, **24**, 6088-6093.

14 P. X. Ma, *Adv Drug Deliv Rev.*, 2008, **60**, 184-198.

15 G. B. Wei and P. X. Ma, *Biomaterials*, 2009, **30**, 6426-6434.

16 G. Chang, H. J. Kim, G. V. Novakovic, D. L. Kaplan and R. Kandel, *J Biomed Mater Res. A*, 2010, **92A** , 43-51.

17 A. Vasconcelos, A. C. Gomes and A. Cavaco-Paulo, *Acta Biomater.*, 2012, **8**, 3049-3060.

18 A. L. Oliveira, L. Sun, H. J. Kim, X. Hu, W. Rice, J. Kluge, R. L. Reis and D. L. Kaplan, *Acta Biomater.*, 2012, **8**, 1530-1542.

19 N.A. Guziewicz, A.J. Massetti, B.J. Perez-Ramirez and D.L. Kaplan, *Biomaterials*, 2013, **34**, 7766-7775.

20 S. Hofmann, C.T. Foo, F. Rossetti, M. Textor, G. Vunjak-Novakovic, D.L. Kaplan, H.P. Merkle and L. Meinel, *J Control Release*, 2006, **111**, 219-227.

21 E. Wenk, A.J. Wandrey, H.P. Merkle and L. Meinel, *J Control Release*, 2008, **132**, 26-34.

22 R. Nazarov, H. J. Jin and D. L. Kaplan, *Biomacromolecules*, 2004, **5**, 718-726.

23 Q. Lu, X. L. Wang, S. Z. Lu, M. Z. Li, D. L. Kaplan and H. S. Zhu, *Biomaterials*, 2011, **32**, 1059-1067.

24 Q. Lv, K. Hu, Q. Feng and F. Cui, *J Biomed Mater Res A*, 2008, **84**, 198-207.

25 K. Zhang, Y. Qian, H. Wang, L. Fan, C. Huang, A. Yin and X. Mo, *J Biomed Mater Res A*, 2010, **95**, 870-881.

26 Q. Zhang, P. Dong, L. Chen, X. Wang and S. Lu, *J Biomed Mater Res A*, 2013, **102**, 76-83.

27 R. Nazarov, H.J. Jin and D.L. Kaplan, *Biomacromolecules*, 2004, **5**, 718-726.

28 H. J. Jin, J. Park, V. Karageorgiou, U. J. Kim, R. Valluzzi, P. Cebe and D. L. Kaplan, *Adv. Funct. Mater*,. 2005, **15**, 1241.

29 Q. Lu, H. S. Zhu, C. Zhang, F. Zhang, B. Zhang and D. L. Kaplan, *Biomacromolecules*, 2012, **13**, 826.

30 S.M. Bai, S. S. Liu, C. C. Zhang, W. A. Xu, Q. Lu, H.Y. Han, D. L. Kaplan and H. S. Zhu, *Acta Biomater.*, 2013, **9(8)**, 7806-7813.

31 Q. Lu, Y. L. Huang, M. Z. Li, B. Q. Zuo, S. Z. Lu, J. N. Wang, H. S. Zhu and D. L. Kaplan, *Acta Biomater.*, 2011, **7**, 2394-2400.

32 Q. Lu, X. H. Zhang, X. Hu and D. L. Kaplan, *Macromol Biosci.*, 2010, **10**, 289-298.

33 T. Xu, W. X. Zhao, J. M. Zhu, M. Z. Albanna, J. J. Yoo and A. Atala, *Biomaterials*, 2013, **34**, 130-139.

34 S. Bollini, M. Pozzobon, M. Nobles, J. Riegler, X. B. Dong, M. Piccoli, A. Chiavegato, A. N. Price, M. Ghionzoli, K. K. Cheng, A. Cabrelle, P. R. Omahoney, E. Cozzi, S. Sartore, A. Tinker, M. F. Lythgoe and P. De Coppi, *Stem Cell Rev Rep.*, 2011, **7**, 364-380.

35 I. Antonucci, A. Pantalone, S. Tete, V. Salini, C. V. Borlongan, D. Hess and L. Stuppia, *Curr Pharm Design*, 2012, **18**, 1846-1863.

36 P. De Coppi, G. Bartsch, M. M. Siddiqui, T. Xu, C. C. Santos, L. Perin, G. Mostoslavsky, A. C. Serre, E. Y. Snyder, J. J. Yoo, M. E. Furth, S. Soker and A. Atala, *Nat Biotechnol.*, 2007, **25**, 100-106.

37 P. H. Chao, S. Yodmuang, X. Wang, L. Sun, D. L. Kaplan and G. Vunjak-Novakovic, *J Biomed Mater Res B Appl Biomater.*, 2010, **95**, 84-90.

38 Q. Lu, X. Hu, X. Q. Wang, J. A. Kluge, S. Z. Lu, P. Cebe and D. L. Kaplan, *Acta Biomater.*, 2010, **6**, 1380-1387.

39 T. Asakura, A. Kuzuhara, R. Tabeta and H.Saito, *Macromolecules*, 1985, **18**, 1841–1845.

40 N. Goujon, R. Rajkhowa, X. Wang and N. Byrne, *J Appl Polym Sci.*, 2013, **128**, 4411-4416.

41 S. Dutta, B. Talukdar, R. Bharal, R. Rajkhowa and D. Dev, *Biopolymers*, 2013, **99**, 326-333.

42 H. Cao, X. Chen, J. R. Yao and Z. Z. Shao, *J Mater Sci*, 2013, **48**, 150-155.

43 Q. Lu, B. Zhang, M. Z. Li, B. Q. Zuo, D. L. Kaplan, Y. L. Huang and H. S. Zhu, *Biomacromolecules*, 2011, **12**, 1080-1086.

44 X. Hu, D. L. Kaplan and P. Cebe, *Macromolecules*, 2006, **39**, 6161-6170.

45 K. Y. Lee and W. S. Ha, *Polymer*, 1999, **40**, 4131-4134.

46 A. Motta, L. Fambri and C. Migliaresi, *Macromol Chem Phys*., 2002, **203**, 1658-1665.

47 X. Hu, D. Kaplan and P. Cebe, *Macromolecules*, 2008, **41**, 3939-3948.

48 M. Pyda, X. Hu and P. Cebe, *Macromolecules*, 2008, **41**, 4786-4793.

49 D. Wilson, R. Valluzzi and D. L. Kaplan, *Biophys.*, 2000, **78**, 2690-2701.

50 X. Hu, K. Shmelev, L. Sun, E. S. Gil, S.H. Park, P. Cebe and D. L. Kaplan, *Biomacromolecules*, 2011, **12**, 1686-1696.

51 Y. Tamada, *Biomacromolecules*, 2005, **6**, 3100-3106.

52 Z. Cao, J. Wen, J. Yao, X. Chen, Y. Ni and Z. Z. Shao, *Mater Sci Eng C*, 2013, **33**, 3522-3529.

53 S. Hofmann, K. S. Stok, T. Kohler, A. J. Meinel and R. Muller, *Acta Biomater.*, 2014, **10**, 308-317

54 A. Atala and P. X. Ma, *Biomaterials*, 2010, **31**, 1133-1139.

55 J. Meyle, H. Wolburg and A.F. von Recum, *J Biomater Appl*, 1993, **7**, 362-374.

56 Y. Song, Y. Ju, G. Song and Y. Morita, *Int J Nanomedicine*, 2013, **8**, 2745-2756.

57 S.J. Florczyk, D.J. Kim, D.L. Wood and M. Zhang, *J Biomed Mater Res A*, 2011, **98**, 614-620.

Captions

Fig. 1 AFM images of silk fibroin solutions on mica surfaces prepared by the repeated drying-dissolving process and SEM images of lyophilized silk scaffolds derived from the solutions: (a) fresh silk fibroin solution, SF-0; (b) scaffolds derived from SF-0, SF-0-S; (c) drying-dissolution once, SF-1; (d) scaffolds derived from SF-1, SF-1-S; (e) drying-dissolution two times, SF-2; (f) scaffolds derived from SF-2, SF-2-S; (g) drying-dissolution three times, SF-3; (h) scaffolds derived from SF-3, SF-3-S, (i) drying-dissolution four times, SF-4, and (j) scaffolds derived from SF-4, SF-4-S. The high magnification SEM images provide the thickness of pore walls of the different scaffolds.

Fig. 2 SEM images of the different scaffolds after incubated in 5 U/ml protease XIV solution for 8 h: (a) SF-0-S; (b) SF-1-S; (c) SF-2-S; (d) SF-3-S; (e) SF-4-S. The number indicates the drying-dissolving cycle times. The high magnification SEM images provide the nanostructures of silk fibroin inside the pore walls.

Fig. 3 CD spectra for SF solutions prepared with the drying-dissolving process. SF-0, fresh silk fibroin solution; SF-1, the solution after drying-dissolving cycle one time; SF-2, the solution after drying-dissolving cycle two times; SF-3, the solution after drying-dissolving cycle three times; and SF-4, the solution after drying-dissolving cycle four times.

Fig. 4 (A) FTIR spectra and (B) X-ray diffraction of the scaffolds derived from silk fibroin solutions treated through the drying-dissolving process: (a) scaffolds derived from fresh silk fibroin solution, SF-0-S; (b) scaffolds derived from the solution after drying-dissolving cycle one time, SF-1-S; (c) scaffolds derived from the solution after drying-dissolving cycle two times, SF-2-S; (d) scaffolds derived from the solution after drying-dissolving cycle three times, SF-3-S; and (e) scaffolds derived from the solution after drying-dissolving cycle four times, SF-4-S.

Fig. 5 (A) TMDSC curves of different scaffolds: (a) scaffolds derived from fresh silk fibroin solution, SF-0-S; (b) scaffolds derived from the solution after drying-dissolving cycle one time, SF-1-S; (c) scaffolds derived from the solution after drying-dissolving cycle two times, SF-2-S; (d) scaffolds derived from the solution after drying-dissolving cycle three times, SF-3-S; and (e) scaffolds derived from the solution after drying-dissolving cycle four times, SF-4-S. (B) Viscosity shear rate profiles of different SF solutions at 2.2 wt% concentrations: SF-0, fresh silk fibroin solution; SF-1, the solution after drying-dissolving cycle one time; SF-2, the solution after drying-dissolving cycle two times; SF-3, the solution after drying-dissolving cycle three times; and SF-4, the solution after drying-dissolving cycle four times.

Fig. 6 Mechanism of silk fibroin porous structure formation regulated by the nanofiber in freeze-drying process.

The formed nanofibers entangle in aqueous solution, resulting in the formation of porous structures.

Fig. 7 AFM images of silk fibroin nanofibers (a) and SEM images of the silk fibroin scaffolds derived from silk fibroin solution containing different contents of nanofibers: (b) scaffolds derived from fresh silk fibroin solution, (c) scaffolds derived from silk fibroin solution containing 1% nanofiber, and (d) scaffolds derived from silk fibroin solution containing 10% nanofiber.

Fig. 8 FTIR spectra of the silk fibroin scaffolds after methanol or water-annealing treatments: (a) water annealed SF-0-S, (b) water annealed SF-1-S, (c) water annealed SF-2-S, (d) water annealed SF-3-S, (e) water annealed SF-4-S, (f) methanol annealed SF-0-S, (g) methanol annealed SF-1-S, (h) methanol annealed SF-2-S, (i) methanol annealed SF-3-S, (j) methanol annealed SF-4-S.

Fig. 9 Amniotic fluid-derived stem cells proliferation on silk scaffolds: MT-SF-0-S, methanol-annealed silk fibroin scaffolds derived from fresh silk fibroin solution; MT-SF-4-S, methanol-annealed scaffolds derived from the solution after drying-dissolving cycle four times. Error bars represent mean ± standard deviation with N=5 (*$p < 0.05$).

Fig. 10 Confocal microscopy of amniotic fluid-derived stem cells cultivated on different scaffolds at day 1 and 12: (a) methanol-annealed silk fibroin scaffolds derived from fresh silk fibroin solution, day 1; (b) methanol-annealed scaffolds derived from the solution after drying-dissolving cycle four times, day 1; (c) methanol-annealed silk fibroin scaffolds derived from fresh silk fibroin solution, day 12; and (d) methanol-annealed scaffolds derived from the solution after drying-dissolving cycle four times, day 12. The scaffolds were stained with FITC for cells (green) and DAPI for nuclei and scaffolds (blue).

Fig. 11 SEM images of amniotic fluid-derived stem cells cultivated on different scaffolds at day 1 and 12: (a) methanol-annealed silk fibroin scaffolds derived from fresh silk fibroin solution, day 1; (b) methanol-annealed scaffolds derived from the solution after drying-dissolving cycle four times, day 1; (c) methanol-annealed silk fibroin scaffolds derived from fresh silk fibroin solution, day 12; and (d) methanol-annealed scaffolds derived from the solution after drying-dissolving cycle four times, day 12.

μm

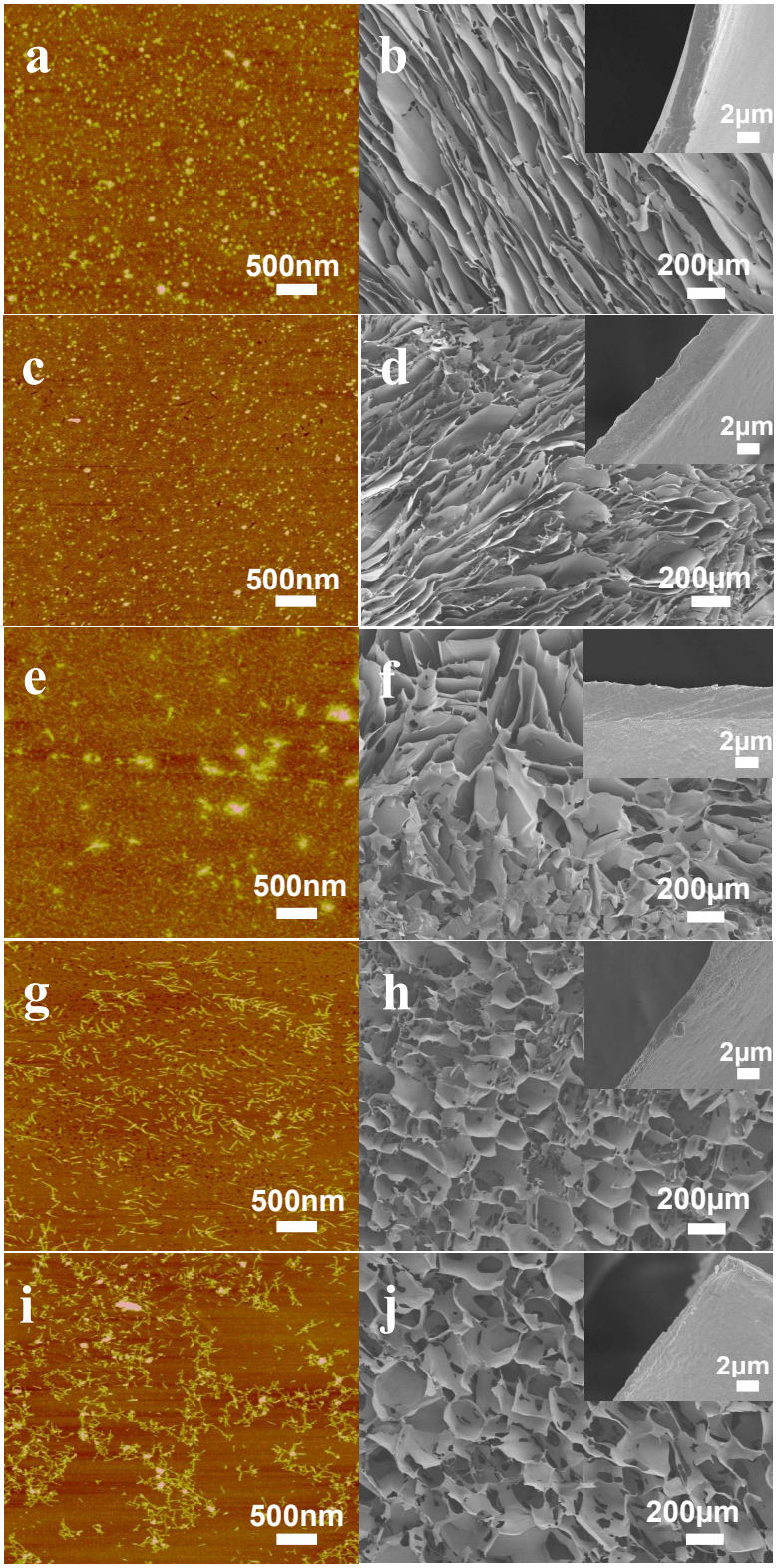

Fig. 1

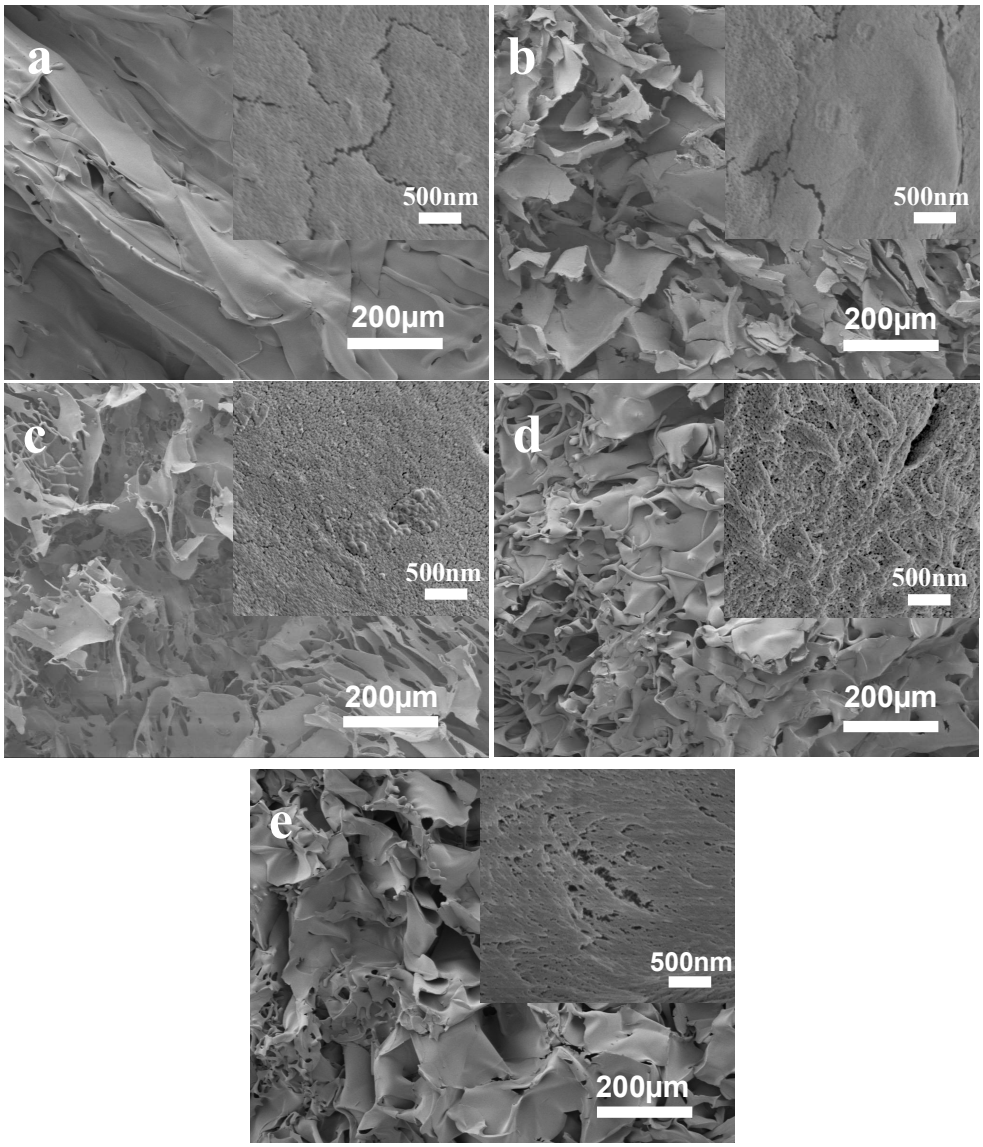

Fig. 2

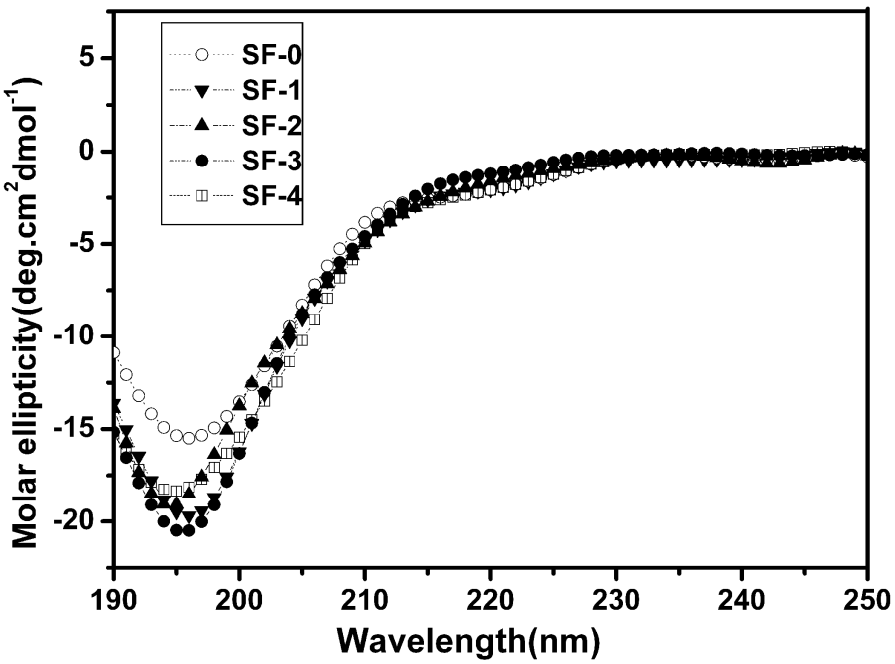

Fig. 3

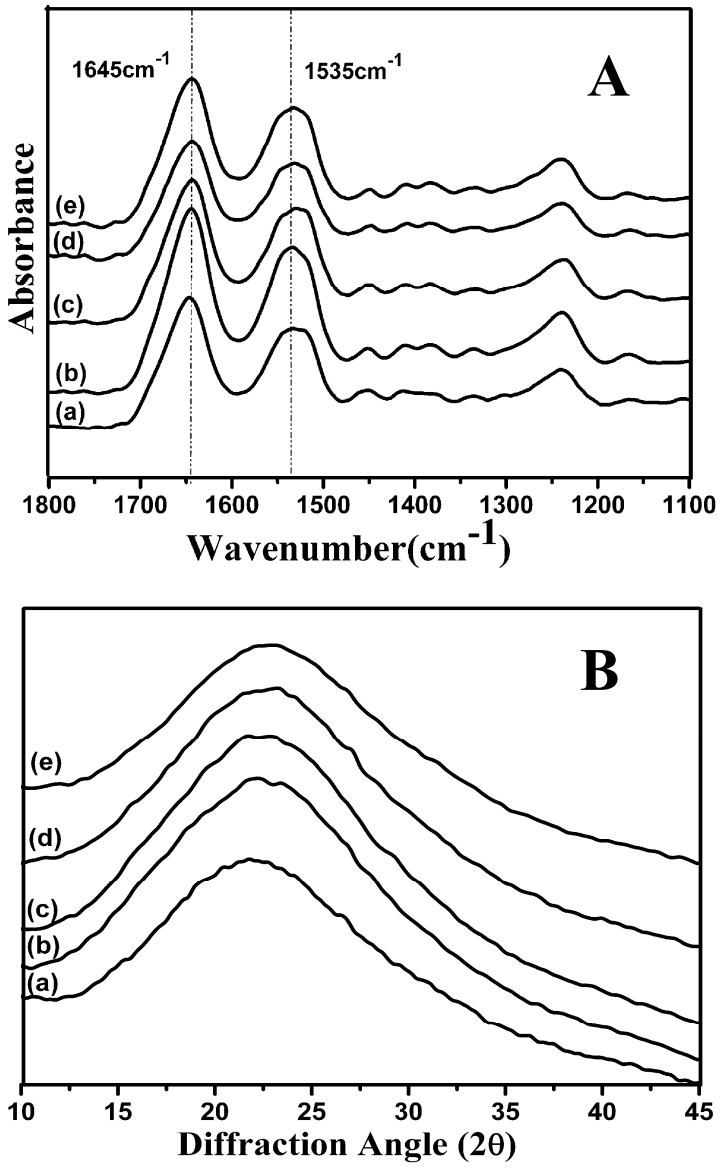

Fig. 4

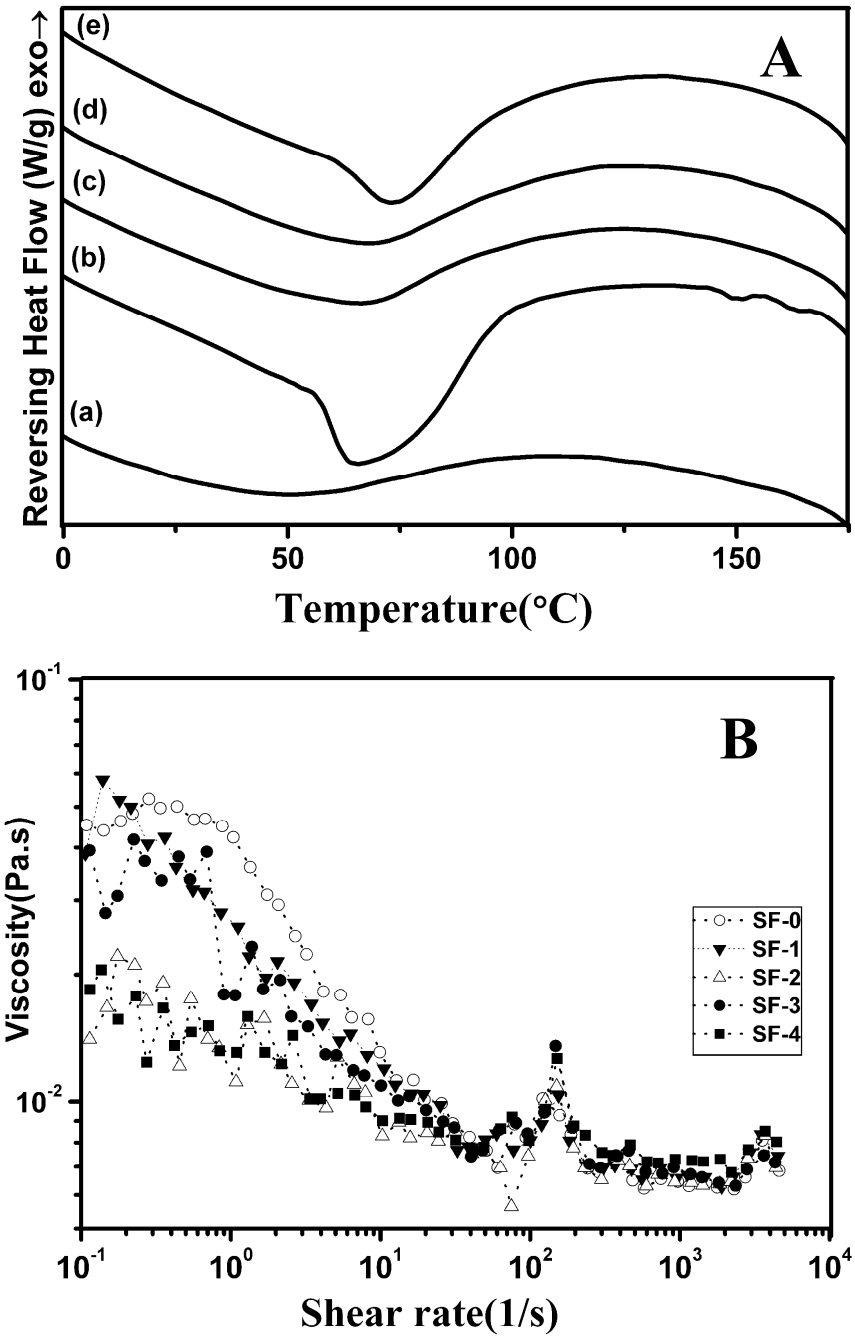

Fig. 5

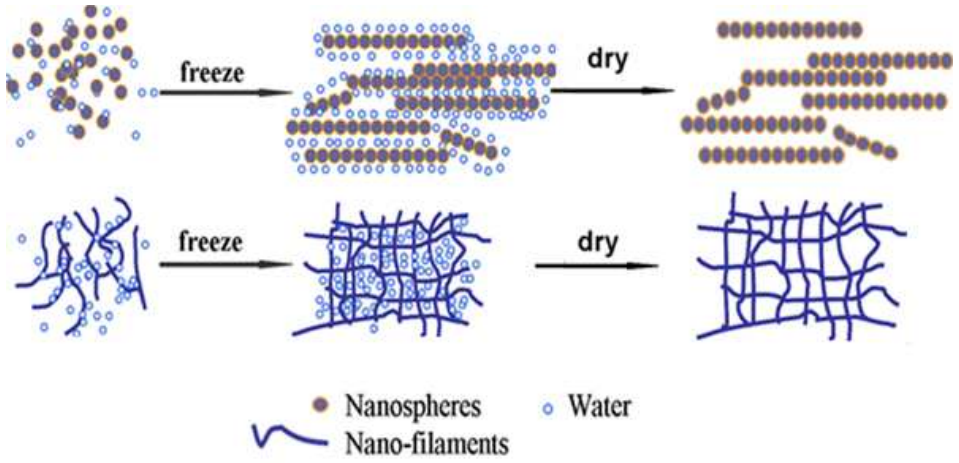

Fig. 6

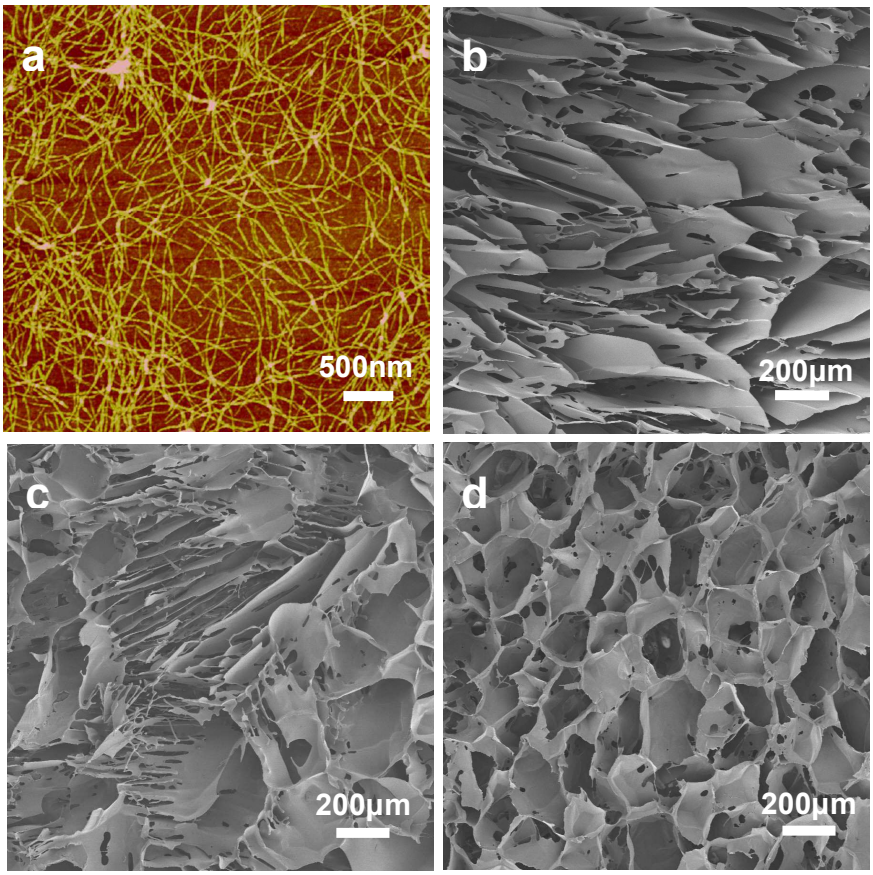

Fig. 7

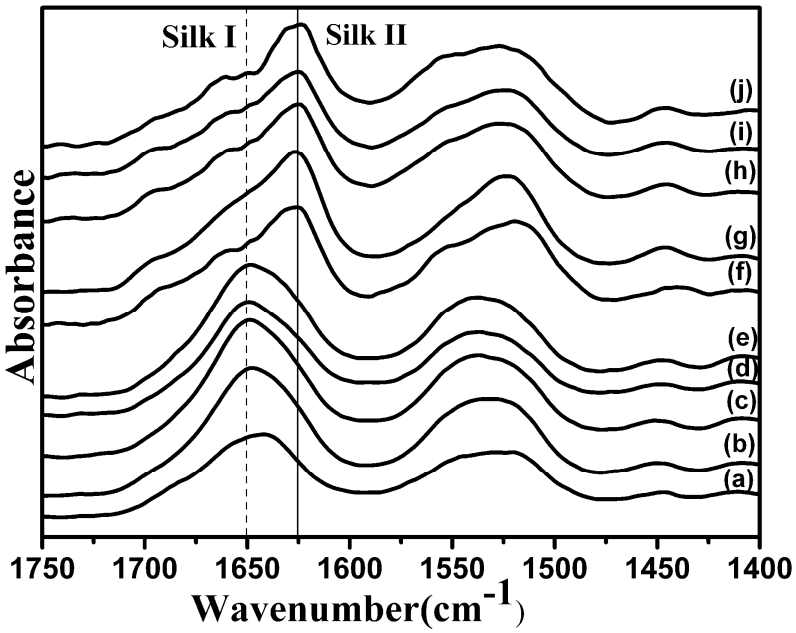

Fig. 8

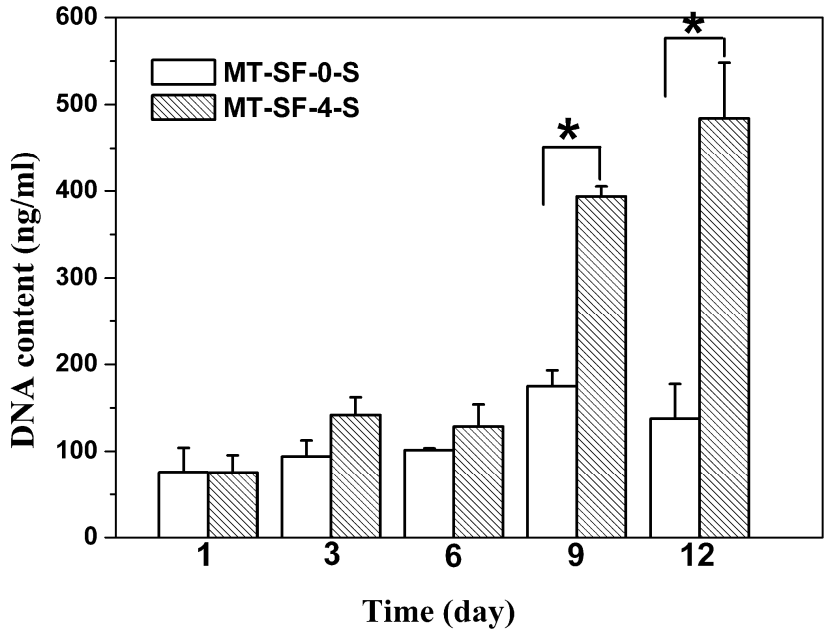

Fig. 9

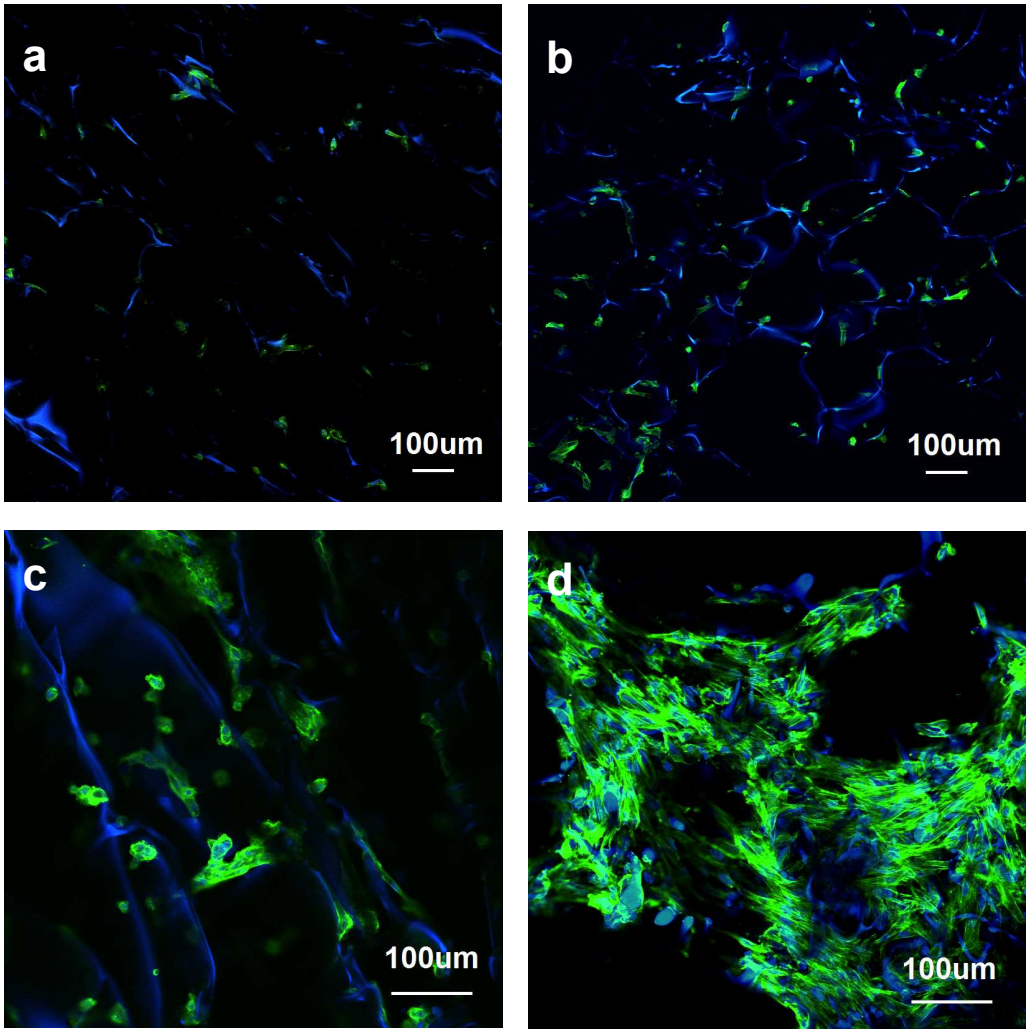

Fig. 10

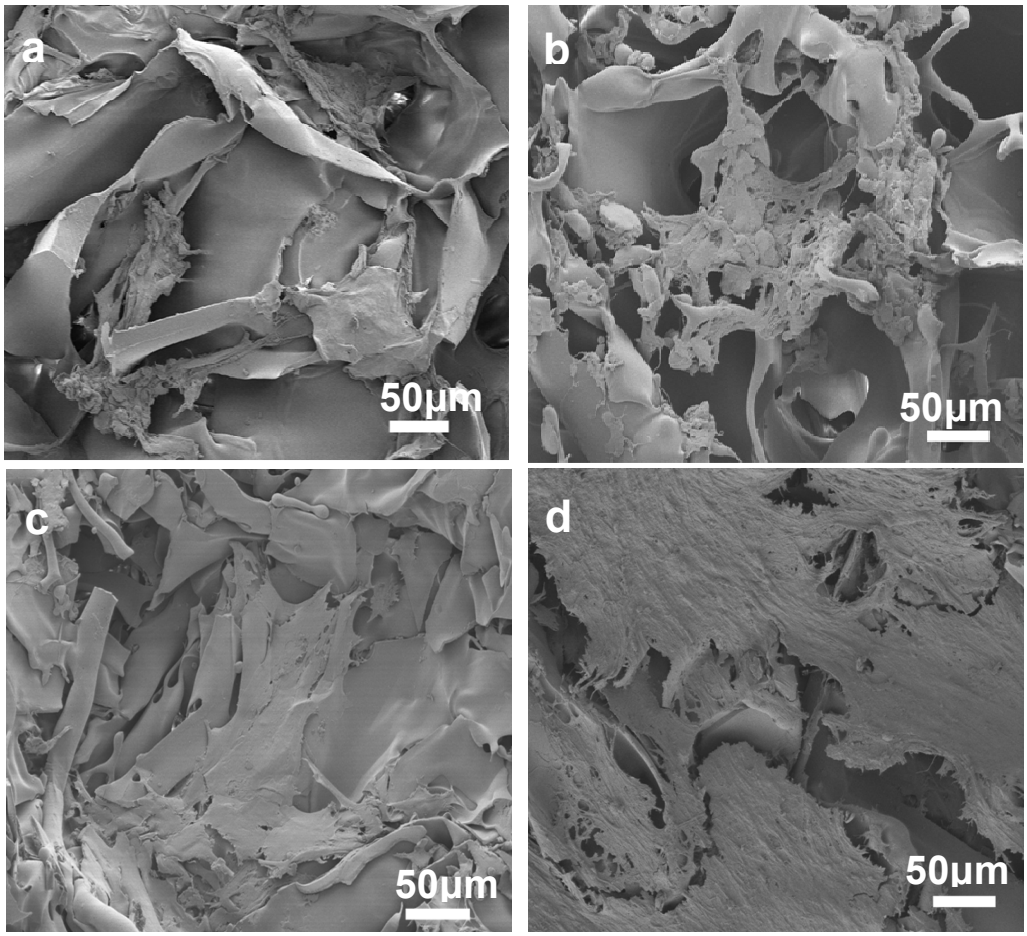

Fig. 11

A Table of Contents Entry

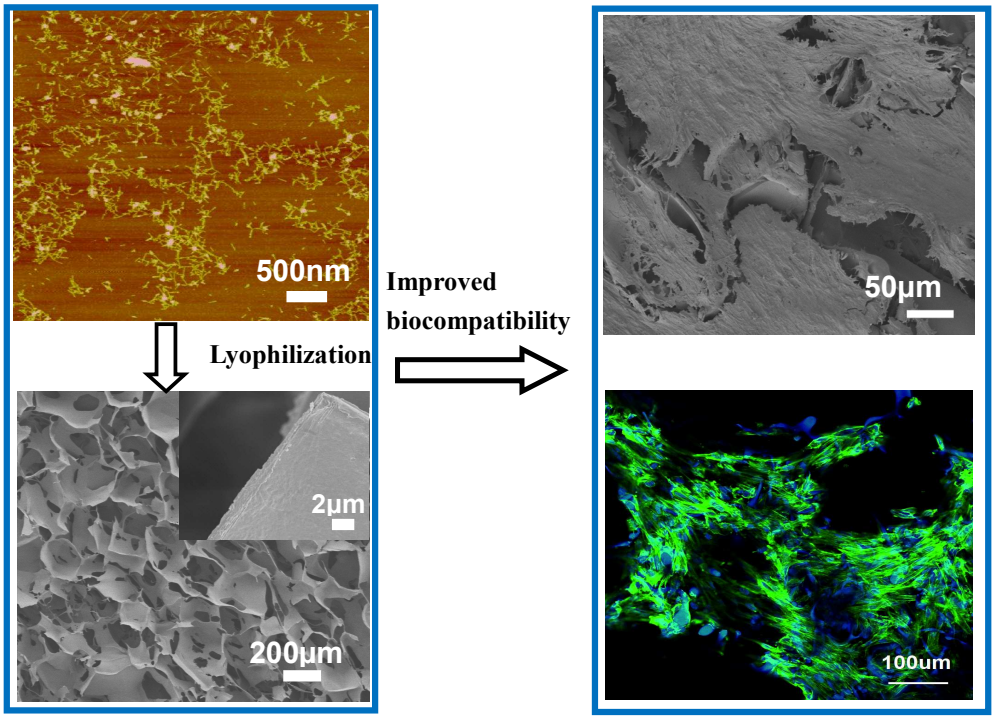

Silk nanofibers were self-assembled in aqueous solution to improve microporous structures of freeze-dried scaffolds and then their biocompatibility.